JPE 13-3-12

http://dx.doi.org/10.6113/JPE.2013.13.3.437

Design of an LCL-Filter for Three-Parallel Operation of Power Converters in Wind Turbines

Hae-Gwang Jeong*, Dong-Keun Yoon**, and Kyo-Beum Lee†

†*Department of Electrical and Computer Engineering, Ajou University, Suwon, Korea
**Research Group, LG Innotek Co., Ltd., Ansan, Korea

Abstract

This paper proposes a design scheme for an LCL-filter used for the three-parallel operation of the power converters in high-capacity wind turbines. The designs of the power devices and grid connected filter are difficult due to the high level voltages and currents in huge-capacity wind turbines. To solve these problem, this paper presents three-parallel operation and LCL-filter design techniques optimized by parallel operation. Furthermore, the design of an inverter side inductance of the LCL-filter is discussed in detail considering the switching modulation method. Simulation and experimental results demonstrate the validity of the designed filter and wind turbines.

Key words: LCL-filter, Power factor compensation, Three-parallel operation, Wind turbine

I. INTRODUCTION

Permanent magnet synchronous generators (PMSGs) are widely used in variable-speed wind turbines due to their high performance. This is due to the fact that they have more optimal characteristics, such as higher efficiency and generated power-weight ratios, than doubly-fed induction generators (DFIGs) [1]. However, the power devices must support high currents to get their high-power rating because PMSGs are connected directly to the grid through a converter [2]-[4]. These topologies are called the full converter type. In these systems, the main issues are the design of the power conversion circuit and grid connected filter.

Many studies have been conducted on the design of high voltage and high current converters. The one solution is the parallel operation of the power devices. When the power devices are connected n- parallel, the rated current of each of the power devices can be reduced to 1/n of the rated value. However, this solution has a problem due to the circulating current caused in each of the legs [5]. On the other hand, the power rating for wind power generation systems is usually high. Therefore, the switching frequency of the converter is restricted to 1~3kHz [6]. This relatively low switching frequency may result in an increase in the harmonics found in the output current. These harmonics can have a negative influence on other sensitive loads and equipment on the grid. According to the IEEE Std 519-1992, the harmonic current distortion on power systems 69kV and below is limited to 5% of the total harmonic distortion (THD). Specifically, the 23th and higher order harmonic current distortions are limited to 0.6% or below the individual harmonic distortions [7], [8]. Therefore, it is necessary to design a filter to reduce the harmonic current distortions of the switching frequency. The inductance of the power conversion devices has conventionally been used to reduce these harmonics. However, since the capacity of systems has been increasing, high values of the inductances are needed. As a result, realizing practical filters has been becoming even more difficult due to rising prices and poor dynamic responses. Therefore, it is necessary to minimize the inductance and to effectively decrease the harmonic current distortions of the switching frequency in designing filters [9], [10]. The problems caused by realizing practical L-filters in high power systems, such as several MW-wind turbines, can be solved by using LCL-filters. An additional LC-part can effectively reduce the harmonics in high frequencies. The increase in the capacitance makes the performance of the filters more effective. To increase the capacitance, it is recommended to use a delta connected LCL-filter because the single equivalent capacitance is increased 3 times the value of delta connected capacitors. Previous studies on the design of

Manuscript received Jul. 16, 2012; revised Apr. 4, 2013
Recommended for publication by Associate Editor Jinjun Liu.
†Corresponding Author: kyl@ajou.ac.kr
Tel: +82-31-219-2376, Fax: +81-31-212-9531, Ajou University
*Dept. of Electrical and Computer Eng., Ajou University, Korea
**LG Innotek Co.,Ltd., Ansan, Korea

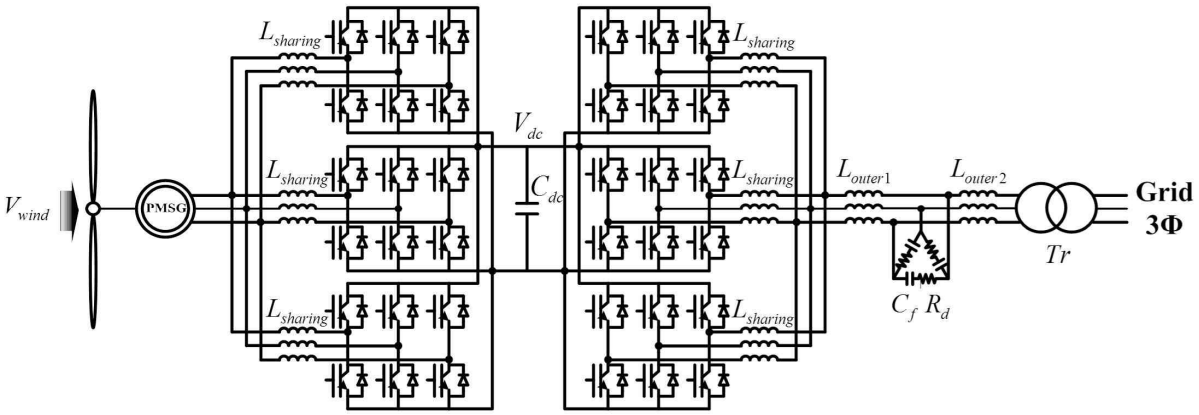

Fig. 1. The three-parallel power converter for wind turbines.

LCL-filters usually focus on the additional LC-part design considering the effects of all the elements [11]-[13]. In these papers, the investigation of the design of an inner inductor was not handled in depth. In [11], the inner inductor design is not mentioned in the body of the text, and in [12] the inner inductance is designed empirically. [13] presented a design method for the inner inductance but this technique does not consider the modulation method.

In this paper, a design method for delta connected LCL-filters is proposed, which includes a shared inductance for the prevention of the circulating current that can be caused by using three-parallel operation. A novel design method for the inner inductance of the LCL-filter is proposed in order to reduce the existing trial and error methods used in exactly designing filters to meet the rated conditions of systems and the required current ripple limits at the point of common coupling (PCC). The presented design technique includes the consideration of the SVM method that is mostly applied to three phase converters. Simulation and experimental results show that the proposed methods are effective and feasible for three-parallel operation in high-power wind systems.

II. THE PMSG WIND SYSTEM

A. The Control for the Parallel Operation

Fig. 1 shows a three-parallel power converter for wind turbines. Each inverter can be controlled independently (an inner control) or together (an outer control). In the case of an inner control, all of the currents in each leg should be measured and circulating currents occur because each inverter has a different switching state. This outer method uses a d-q current controller to make the same reference voltages applied into each of the branches [2].

The PI gains of the current controller are determined by the parameters of the LCL-filter and grid impedance in (1).

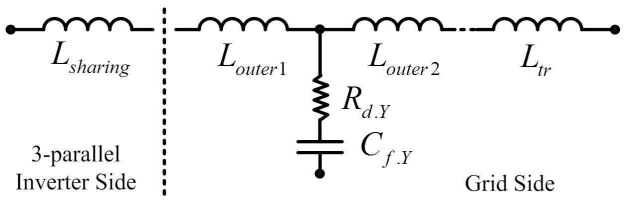

Fig. 2. The equivalent circuit of the LCL-filter for a parallel operation converters.

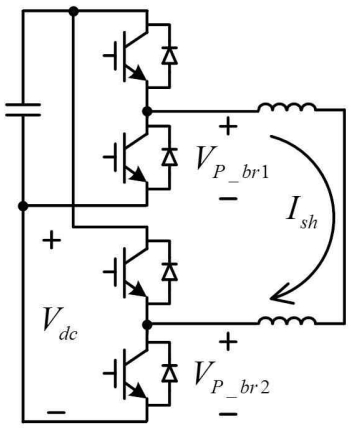

(a)

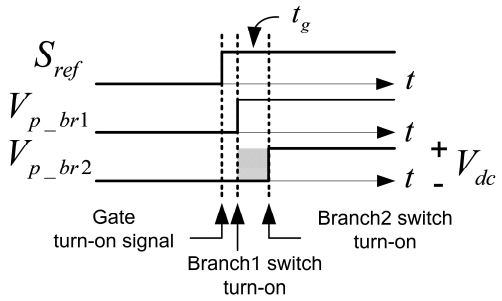

(b)

Fig. 3. The analysis of the circulating current (a) an equivalent circuit of 2-leg switches (b) the voltage deference caused by interval of the switching turn-on time between the parallel branches.

$$L_i = L_{sharing}/3 + L_{outer1} + L_{outer2} + L_{tr}$$
$$K_P = L_i \cdot \omega_c \quad (1)$$
$$K_i = R_i \cdot \omega_c$$

where L_i is the equivalent inductance and R_i is the equivalent resistance in the converter.

In the outer control method, all of the corresponding switches of the parallel converter units are turned on and off at the same time. Circulating current does not occur because there is no voltage difference between the parallel branches in the ideal condition.

B. The Topology of the Filter for the Three-parallel Power Converter

A delta connected LCL-filter is connected to the three-parallel power converter with consideration of the large filter volume, as shown in Fig. 2.

The inner inductance is divided into the outer1 inductance and the three-parallel sharing inductance, which prevents circulating currents from occurring by using the short circuit inherent in the parallel branches.

The time interval of the switching turn-on time can make a short circuit between the parallel branches. When the switching turn-on signal (S_{ref}) is transmitted to both of the switches of branch 1 and branch 2, the difference in the voltage between the pole voltages of branch 1 ($V_{p\text{-}br1}$) and branch 2 ($V_{p\text{-}br2}$) becomes the DC-link voltage (V_{dc}), because the turn-on times of the switches are different, as shown Fig. 3. The circulating current is determined by an internal variable of the converter as the DC-link voltage, the interval of the switching turn-on or-off time of each leg and the inductance of the sharing reactor because the circulating current flows only through the parallel circuit of the power conversion part.

$$L_{sharing} \geq \frac{V_{dc} t_g}{2 i_{sh\_\max}} \quad (2)$$

where t_g is the period of the worst-case switching interval between the parallel branches, as seen in Fig. 3. This can be determined by a datasheet of the power devices.

As shown in (2), the sharing inductance can be designed to meet a permitted circulating current (i_{sh_max}). The values of the sharing inductors of the machine side converter and the grid side converter are the same.

In order to design this filter, a single-phase equivalent circuit of this filter is used, as shown in Fig. 2. The parameters for the design are defined as:

$$L_1 = \frac{1}{3} L_{sharing} + L_{outer1}$$
$$L_g = L_{outer2} + L_{tr}$$
$$C_{f.Y} = 3C_{f.\Delta} \quad (3)$$
$$R_{d.Y} = \frac{1}{3} R_{d.\Delta}$$

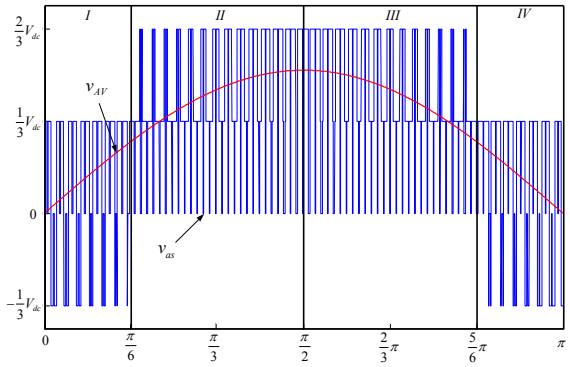

Fig. 4. The output phase voltage (v_{as}) and average voltage (v_{AV}) when $Mi = 0.89$.

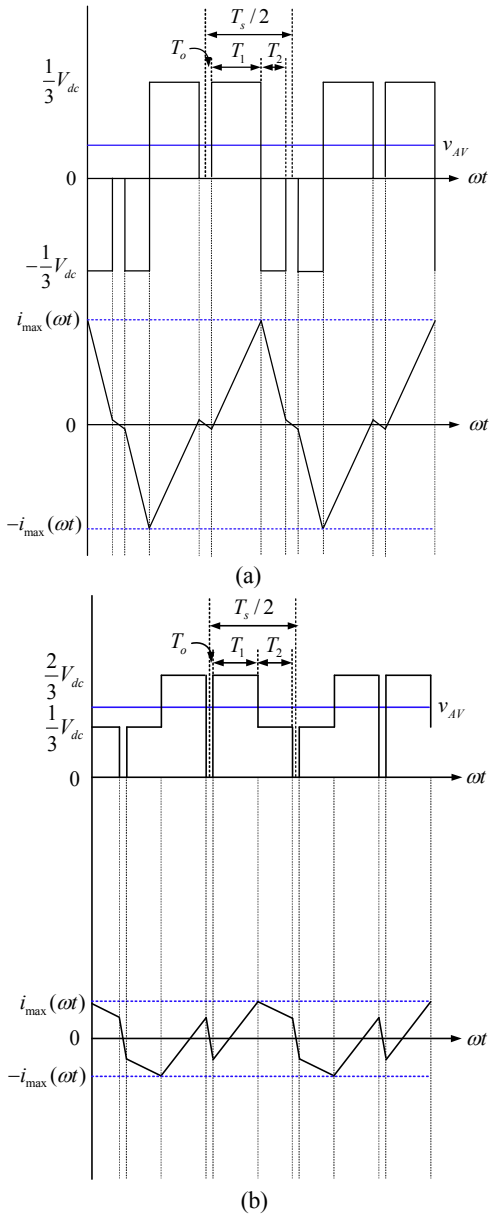

Fig. 5. The current ripples at each region (a) at the I and IV regions and (b) at the II and III regions.

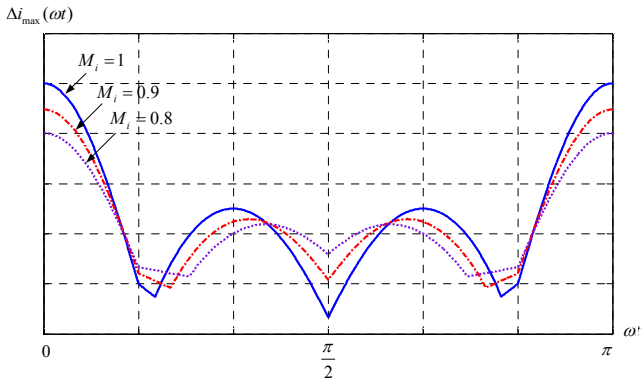

Fig. 6. The magnitude of the current ripples according to the modulation index.

TABLE I
THE VALID TIMES AT EACH REGION ACCORDING TO THE LEVEL OF THE OUTPUT PHASE VOLTAGE

Region	Output phase voltage	Valid time	
I	0	T_0	T_b
	$1/3V_{dc}$	T_1	T_a - T_b
	$-1/3V_{dc}$	T_2	T_c - T_a
II	0	T_0	T_b
	$2/3\ V_{dc}$	T_1	T_a - T_c
	$1/3\ V_{dc}$	T_2	T_c - T_b
III	0	T_0	T_c
	$2/3\ V_{dc}$	T_1	T_a - T_b
	$1/3\ V_{dc}$	T_2	T_b - T_c
IV	0	T_0	T_c
	$1/3\ V_{dc}$	T_1	T_a - T_c
	$-1/3\ V_{dc}$	T_2	T_b - T_a

where $L_{sharing}$, L_{outer1}, L_{outer2}, L_{tr}, $C_{f\Delta}$, and $R_{d\Delta}$ are the sharing inductor of each branch, the inductor between the sharing inductor and the capacitor, the inductor between the capacitor and the transformer, the inner inductor of the transformer, the delta connected capacitor, and the damping resistor, respectively. The parameters based on this equivalent circuit can be determined by using the design method of the Y connected LCL-filter.

III. DESIGN OF THE DELTA CONNECTED LCL-FILTER

The influence the ripple current has on the power quality can be evaluated by the ripple factor (RF). The ripple factor is defined as the rate of the fundamental current and the switching ripple current.

$$RF = \frac{I_{ripple}(h_{sw})}{I_{rate}} \tag{4}$$

where I_{ripple} is the RMS value of the switching ripple current and I_{rate} is the RMS value of the rated current.

A. The Design of the Inner Inductance (L_1)

Because the inner inductance (L_1), determined by the converter side ripple rate of the LCL-filter, is based on the outer inductance (L_g), the inner inductance must be designed exactly in order to reduce the trial and error in the filter design. The three-phase converter usually uses Third Harmonics Injected Modulation. Its output phase voltages produce current ripples which are very different from those of the single-phase converter. Therefore, the novel design method of the L-filter can be derived through analyzing the current ripple of the inductance.

When the modulation index is unity, the max value of the phase voltage is $V_{dc}/\sqrt{3}$ by Space Vector Pulse Width Modulation (SVPWM). In this paper, instead of triangular waves, third order harmonic sine waves are injected into the neutral point for convenience. Therefore, the pole voltages of the three-phase converter are expressed as:

$$\begin{aligned} v_{an}(\omega t) &= M_i \frac{V_{dc}}{\sqrt{3}}\left[\sin(\omega t) + \frac{1}{6}\sin(3\omega t)\right] \\ v_{bn}(\omega t) &= M_i \frac{V_{dc}}{\sqrt{3}}\left[\sin\left(\omega t - \frac{2}{3}\pi\right) + \frac{1}{6}\sin(3\omega t)\right] \\ v_{cn}(\omega t) &= M_i \frac{V_{dc}}{\sqrt{3}}\left[\sin\left(\omega t + \frac{2}{3}\pi\right) + \frac{1}{6}\sin(3\omega t)\right] \end{aligned} \tag{5}$$

The valid time, the ON half time of the switch elements is determined by the pole voltages in (5).

The output phase voltages have five-level voltages, such as $2/3V_{dc}$, $1/3V_{dc}$, 0, $-1/3V_{dc}$, and $-2/3V_{dc}$, that are different from those of the single-phase converter found in Fig. 4, because the level of the output phase voltage applied to the load is continuously changing according to variations of each phase valid time. Fig. 4 shows the average voltage (v_{AV}) and the output phase voltage (v_{as}) applied to the load when the modulation index is 0.89.

$$\begin{aligned} T_a &= \frac{T_s}{2}\left\{\frac{1}{2} + \frac{M_i}{\sqrt{3}}\left[\sin(\omega t) + \frac{1}{6}\sin(3\omega t)\right]\right\} \\ T_b &= \frac{T_s}{2}\left\{\frac{1}{2} + \frac{M_i}{\sqrt{3}}\left[\sin\left(\omega t - \frac{2}{3}\pi\right) + \frac{1}{6}\sin(3\omega t)\right]\right\} \\ T_c &= \frac{T_s}{2}\left\{\frac{1}{2} + \frac{M_i}{\sqrt{3}}\left[\sin\left(\omega t + \frac{2}{3}\pi\right) + \frac{1}{6}\sin(3\omega t)\right]\right\} \end{aligned} \tag{6}$$

If the average voltage and the grid phase voltage (e_{as}) are the same wave as determined by (7) then:

$$v_{AV}(\omega t) = M_i \frac{V_{dc}}{\sqrt{3}}\sin(\omega t) = e_{as}(\omega t) \tag{7}$$

where $0 < \omega t < \pi$.

Thus, the magnitude of the current ripples in each region can be estimated through the times applied into the inductor and the potential of the average voltage and the output phase voltage.

In the I and IV regions, the levels of the output phase voltage are determined to be 0 V for T_0, $1/3V_{dc}$ for T_1 and $-1/3V_{dc}$ for T_2,

as shown in Fig. 5-(a). The magnitude of the current ripples ($\Delta i_{max1,4}$) is determined by the current variations for T_0 and T_1. In the II and III regions, the levels of the output phase voltage are determined to be 0 V for T_0, $2/3V_{dc}$ for T_1, and $1/3V_{dc}$ for T_2, as shown in Fig. 5-(b). The magnitude of the current ripples ($\Delta i_{max2,3}$) is determined by the current variations for T_0, T_1 and T_2. However, the current variation is applied to the calculation of the current ripple magnitude only when the average voltage is higher than $1/3V_{dc}$. Therefore, the magnitude of the current ripples can be calculated through the current variation for $T_s/2$ by:

$$\begin{aligned}
\Delta i_{\max 1}(\omega t) &= \frac{1}{L}\left(\frac{1}{3}V_{dc}-v_{AV}(\omega t)\right)\cdot(T_a-T_b)-\frac{1}{L}v_{AV}(\omega t)T_b \\
\Delta i_{\max 2}(\omega t) &= \frac{1}{L}\left(\frac{2}{3}V_{dc}-v_{AV}(\omega t)\right)\cdot(T_a-T_c)-\frac{1}{L}v_{AV}(\omega t)T_b \\
&+\frac{1}{2L}\cdot\left(\sqrt{\left(\frac{1}{3}V_{dc}-v_{AV}(\omega t)\right)^2}+\left(\frac{1}{3}V_{dc}-v_{AV}(\omega t)\right)\right)\cdot(T_c-T_b) \\
\Delta i_{\max 3}(\omega t) &= \frac{1}{L}\left(\frac{2}{3}V_{dc}-v_{AV}(\omega t)\right)\cdot(T_a-T_b)-\frac{1}{L}v_{AV}(\omega t)T_c \\
&+\frac{1}{2L}\cdot\left(\sqrt{\left(\frac{1}{3}V_{dc}-v_{AV}(\omega t)\right)^2}+\left(\frac{1}{3}V_{dc}-v_{AV}(\omega t)\right)\right)\cdot(T_b-T_c) \\
\Delta i_{\max 4}(\omega t) &= \frac{1}{L}\left(\frac{1}{3}V_{dc}-v_{AV}(\omega t)\right)\cdot(T_a-T_c)-\frac{1}{L}v_{AV}(\omega t)T_c
\end{aligned} \tag{8}$$

The magnitude of the current ripples is symmetrical and has different types according to the modulation index (Mi) as shown in Fig. 6.

Therefore, the modulation index is one of the most important factors in determining the magnitude of the current ripples. The high frequency triangular wave is chosen for the model of the current ripples in order to simply calculate the RMS value of the current ripple, because there are many types of current ripples. The RMS values of the triangular wave are calculated from the absolute value of the triangular wave [14]. It is $1/\sqrt{3}$ times the magnitude of the triangular wave. Consequently, the RMS value of the current ripple is calculated by integrating these RMS values in the I and II regions as:

$$I_{ripple}(h_{sw})=\sqrt{\frac{2}{3\pi}\left[\int_0^{\frac{\pi}{6}}\Delta i_{\max 1}^2(\theta)d\theta+\int_{\frac{\pi}{6}}^{\frac{\pi}{2}}\Delta i_{\max 2}^2(\theta)d\theta\right]} \tag{9}$$

When (9) is calculated, the RMS value of the current ripple is determined by (10), and it is expressed by the DC-link voltage (V_{dc}), the switching period (T_s), the inductance (L) and the modulation index (M_i).

In (10), the modulation index and the base inductance (L_b) conditions are found in (11).

$$M_i=\frac{\sqrt{2}E_n}{V_{dc}},\ L_b=\frac{E_n^2}{2\pi f_n P_n} \tag{11}$$

where E_n is the grid line voltage, P_n is the three-phase power, f_n is the grid frequency and f_{sw} is the switching frequency.

The rated current of the system is determined by the RMS value of the phase voltage and the base inductance (Z_b) by:

$$I_{rate}=\frac{M_i V_{dc}}{\sqrt{3}\sqrt{2}Z_b}=\frac{M_i V_{dc}}{2\sqrt{6}\pi f_n L_b} \tag{12}$$

$$RF=\frac{I_{ripple}(h_{sw})}{I_{rate}} \tag{13}$$

Because the switching ripple factor (RF) is the rate of the current ripple ($I_{ripple}(h_{sw})$) over the rated current of the system (I_{rate}), as seen in (13), the inductance of the L-filter can be obtained from (11), (12) and (13), as shown in (14).

The inner inductance (L_1) has the same performance as the inductance (L) of the L-filter at the converter side. Therefore, the L_1 can be obtained from (14) under the same ripple factor.

$$I_{ripple}(h_{sw})=\frac{V_{dc}M_i T_s}{2\sqrt{3}L}\sqrt{\frac{[\,g_1(M_i)+g_2(M_i)+g_3(M_i)\,]}{699840\pi M_i^4}} \tag{10}$$

where:

$$\begin{aligned}
g_1(M_i)&=\sqrt{3M_i^2-4\sqrt{3}M_i+4}\cdot(3375M_i^5-4014\sqrt{3}M_i^4+1692M_i^3+1128\sqrt{3}M_i^2+96M_i+64\sqrt{3}) \\
g_2(M_i)&=\sqrt{3M_i^2-2\sqrt{3}M_i+1}\cdot(-41040M_i^5+31248\sqrt{3}M_i^4-7632M_i^3-2544\sqrt{3}M_i^2-384M_i-128\sqrt{3}) \\
g_3(M_i)&=(-114480M_i^4)\cdot(\sqrt{3}M_i^2-\frac{163}{212}\pi M_i^2+\frac{12}{53}\sqrt{3}M_i+\frac{459}{530}M_i+\frac{9}{53}\sqrt{3}-\frac{33}{106}\pi)
\end{aligned}$$

$$L=\frac{L_b}{RF}\frac{f_n}{f_{sw}}\sqrt{\frac{2\pi[\,g_1(M_i)+g_2(M_i)+g_3(M_i)\,]}{699840M_i^4}} \tag{14}$$

where:

$$\begin{aligned}
g_1(M_i)&=\sqrt{3M_i^2-4\sqrt{3}M_i+4}\cdot(3375M_i^5-4014\sqrt{3}M_i^4+1692M_i^3+1128\sqrt{3}M_i^2+96M_i+64\sqrt{3}) \\
g_2(M_i)&=\sqrt{3M_i^2-2\sqrt{3}M_i+1}\cdot(-41040M_i^5+31248\sqrt{3}M_i^4-7632M_i^3-2544\sqrt{3}M_i^2-384M_i-128\sqrt{3}) \\
g_3(M_i)&=(-114480M_i^4)\cdot(\sqrt{3}M_i^2-\frac{163}{212}\pi M_i^2+\frac{12}{53}\sqrt{3}M_i+\frac{459}{530}M_i+\frac{9}{53}\sqrt{3}-\frac{33}{106}\pi)
\end{aligned}$$

B. The Design of the Wye Connected Capacitor ($C_{f.Y}$)

The value of the wye connected capacitor is calculated through a percentage (x) of the reactive power absorbed under the rated conditions as determined by (15). From the determined $C_{f.Y}$, the delta connected $C_{f.\Delta}$ is calculated by (3).

$$C_b = \frac{P_n}{2\pi f_n E_n^2}$$
$$C_{f.Y} = xC_b. \quad (15)$$

C. The Design of the Outer Inductance (L_g)

The inductance rate (r) is determined through the relationship between the outer current ripple and the inner current ripple. The relationship between the outer inductance and the inner inductance can also be determined by using the inductance rate (16) [11]. From the determined L_g and L_{tr}, the value of L_{outer2} is calculated by (3).

$$L_g = rL_1. \quad (16)$$

D. The Damping Resistance Calculation ($R_{d.Y}$)

The damping resistance needed to remove the resonance is equal to one third of the impedance of the capacitor in the resonant frequency, and it is calculated with (17). From the determined $R_{d.Y}$, the delta connected $R_{d.\Delta}$ is calculated by (3).

$$f_{res} \cong \frac{1}{2\pi}\sqrt{\frac{L_1 + L_g}{L_1 L_g C_{f.Y}}}$$
$$R_{d.Y} = \frac{1}{6\pi f_{res} C_{f.Y}} \quad (17)$$

where f_{res} is the resonance frequency.

IV. Design Example

The example is designed for the LCL-filter of 2MW wind turbines. The specifications of the system are shown in Table 2. Specifically, the required ripple factor is determined to be 1% in accordance with IEEE Std 519-1992 because the switching frequency is selected as 2kHz in this example.

TABLE II
The Design Specifications of the LCL-filter for the 2MW Wind System

Rated output power	2 MW
Grid line-to-line voltage	690 Vrms
DC-link voltage	1200 V
Grid frequency	60 Hz
Switching frequency	2000 Hz
Worst-case switching gap	1 μs
Permitted circulating current	25 A
Inner inductance of transformer	25 μH
Required ripple factor	< 1 %

TABLE III
The Parameters of Designed LCL-filter

$L_{sharing}$	20μH
L_{outer1}	75.30μH
$C_{f.\Delta}$	371μF
L_{outer2}	67.6μH
$R_{d.\Delta}$	0.19Ω
f_{res}	723Hz

To achieve the required ripple factor, the primary ripple factor is chosen as 10% in the rated condition. The inner inductance can be determined to be 82μH using these parameters and the formulas in section 3.B. When the inner inductance is designed, the $L_{sharing}$ to reduce the circuiting current should be considered. In this example, t_g is decided to be 1μs, and i_{sh_max} is selected to be 1% of rated current. Under these conditions, the sharing reactor is designed to 20μH and L_{outer1} is determined to 75.3μH. For the design of the filter capacitor, x is selected as 10%. The value of x is limited to 5% of the system total impedance in [11], but a large capacitance is applied for the minimization of the filter inductance. Under this condition, the value of the filter capacitor is 1100μF. The value of the filter capacitor is modified to be 371μF due to the application of the delta-connection. Finally, the outer inductance is designed using the previously designed inner inductance and filter capacitance. r in (16) is determined to be 1.13, and the value of the outer inductance is 75.3μH. The parameters of the designed LCL-filter are presented in Table 3.

V. Simulation Results

To confirm the validity of the designed LCL-filter and wind turbines, the simulation of a 2MW wind system has been performed using PSIM.

Fig. 7 shows the performance of the designed inner inductance. In section 4, the inner inductance is designed to achieve a 10% ripple factor. In Fig. 7, the RMS value of the fundamental frequency component of the current is 1670A, and the switching harmonics component is almost 170A. Under this condition, the ripple factor is determined to be 0.1, as shown in Fig. 7(b). These results show that the inner inductance was accurately designed.

The performance of the designed LCL-filter is shown in Fig. 8. The ripple factor of the grid side current is 0.01, as shown in Fig. 8(b). The value of the additional LC part is selected based on the correctly designed inner inductance. Although the total inductance of the designed LCL-filter was 15.02% of the L-filter, this LCL-filter is efficient in eliminating the harmonics of the output current. Its total harmonics distortion (THD) was approximately 1%.

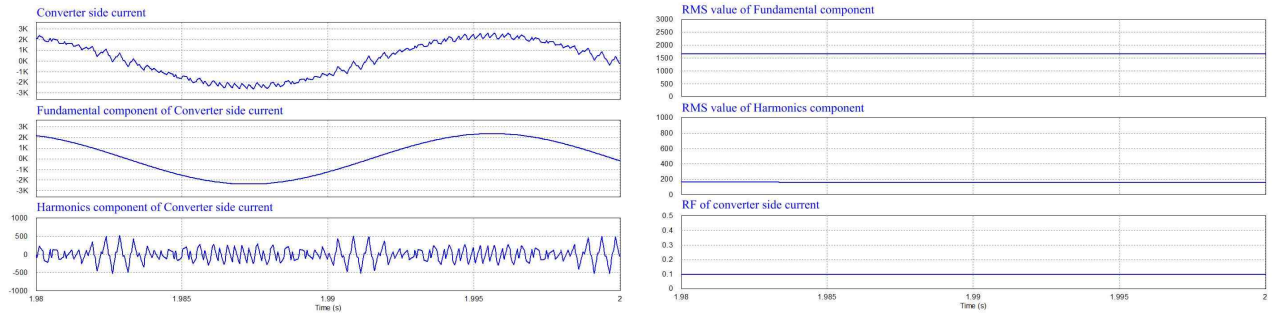

(a) (b)

Fig. 7. The analysis of the harmonics in the inverter side current (a) phase current and its ripple and (b) ripple factor of the phase current.

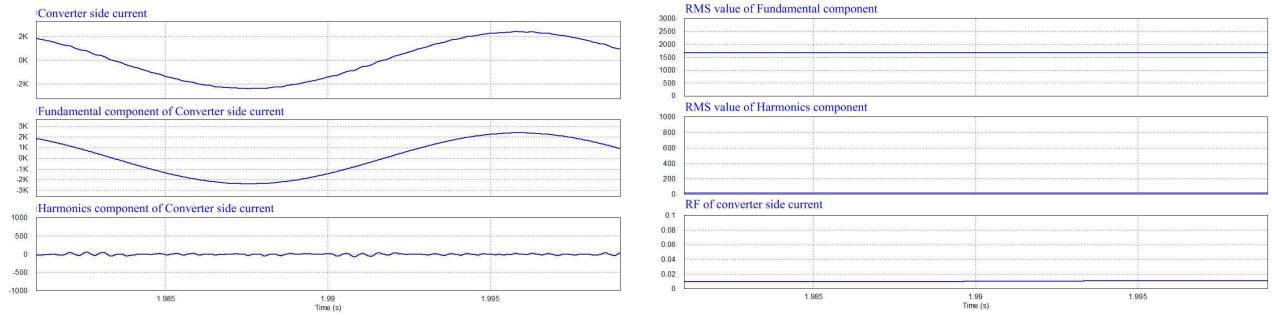

(a) (b)

Fig. 8. The analysis of the harmonics in the grid side current (a) phase current and its ripple and (b) ripple factor of the phase current.

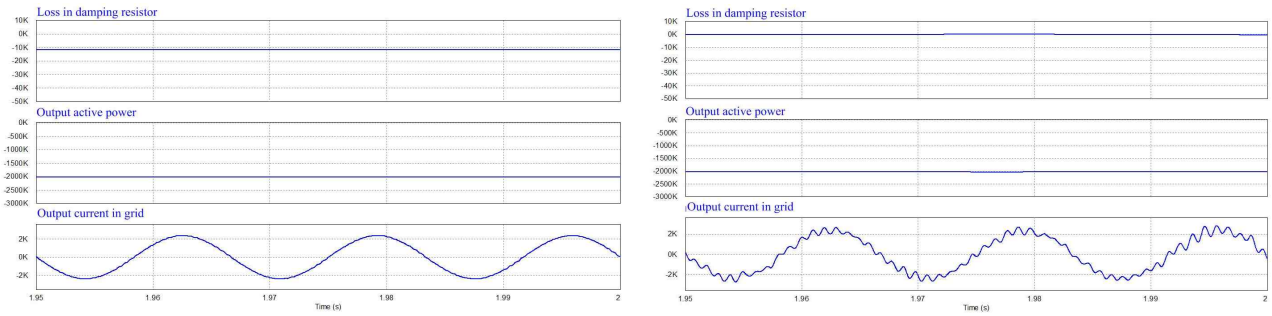

(a) (b)

Fig. 9. Characteristic of the damping resistor (a) with passive damping and (b) without damping.

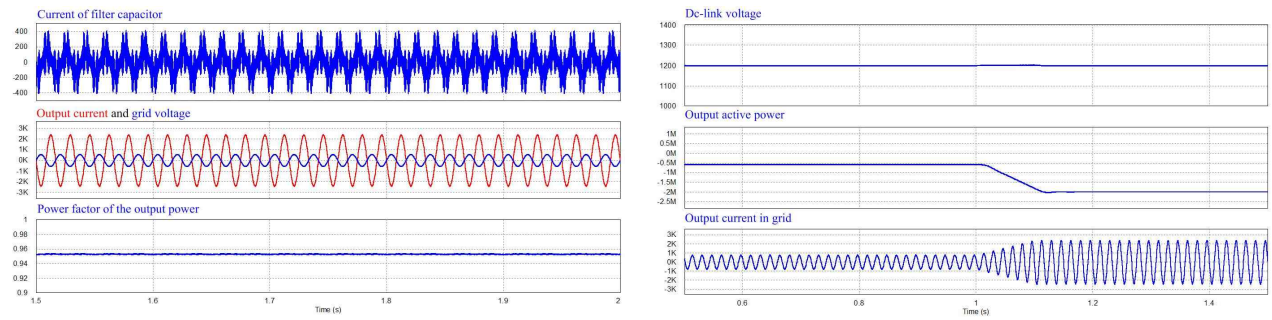

Fig. 10. Effect of the power factor by the filter capacitor.

Fig. 11. The dynamic performance of the grid-side converter.

The damping of the LCL-filter is an issue which cannot be obtained in the performance verification of the LCL-filter. Fig. 9(a) shows the characteristic of the damping resistor. The damping resistor generates a loss of 0.9% and it becomes heat. It results in an unintended loss and causes an additional cost for the cooling system. However, the system can be unstable, if the a damping method is not applied, as shown in Fig. 9(b). In Fig. 9(b), there is no loss caused by the damping resistor but the output current is oscillated by a resonance frequency.

Fig. 10 shows the effect of the power factor by the filter capacitor. The designed LCL-filter has a large capacitance for the reduction of the inductance. Consequently, there is a large fundamental frequency component in the current of the filter capacitor and the power factor decrease to 0.95, as shown in Fig. 10. However, this output is the leading power factor and the reactive power can be compensated by the inverter control.

Fig. 11 shows the dynamic characteristic of the grid connected inverter with the designed LCL-filter. At 1s, the input power of the generator side converter increases from 500kW to 2MW. While the generated power is increased to 2MW, the DC-link voltage was kept at around 1200V and the output current is generated stable without resonance in the dynamic condition.

VI. Experimental Results

The 2MW system explained above has been scaled down to a 10kW system for the experimental purposes. Under this condition, the LCL-filter is designed according to Table 5 using the same procedure as section 4.

TALBE IV
THE DESIGN SPECIFICATIONS OF THE LCL-FILTER 10KW SYSTEM

Rated output power	10 kW
Grid line-to-line voltage	380Vrms
DC-link voltage	600 V
Grid frequency	60 Hz
Switching frequency	2000 Hz
Worst-case switching gap	1 μs
Permitted circulating current	0.15 A
Inner inductance of transformer	Ignore
Required ripple factor	< 1 %

TABLE V
THE PARAMETERS OF DESIGNED LCL-FILTER FOR THE EXPERIMENTAL SET-UP

$L_{sharing}$	2mH
L_{outer1}	2mH
$C_{f\Delta}$	7.35μF
L_{outer2}	1.28mH
f_{res}	734Hz
$R_{d\Delta}$	6.3Ω

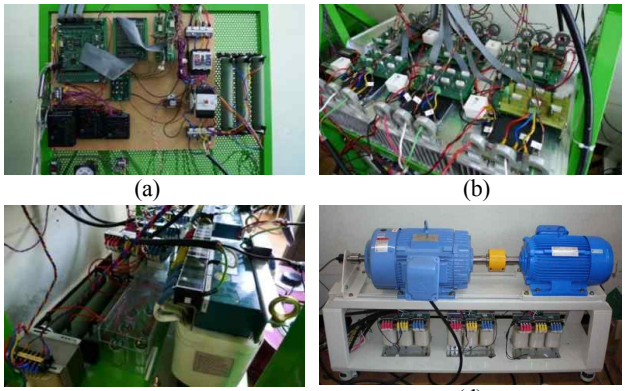

Fig. 12. The experimental setup (a) DSP controller board, (b) Three-parallel power converters, (c) LCL-filter and (d) MG-set.

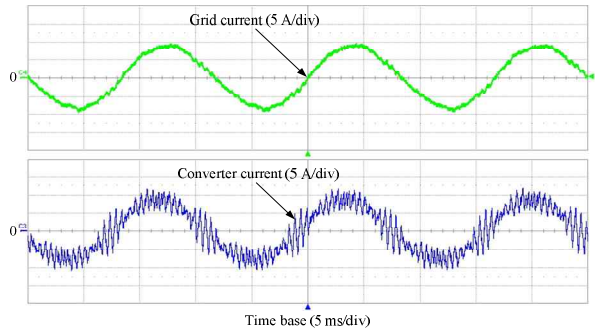

(a)

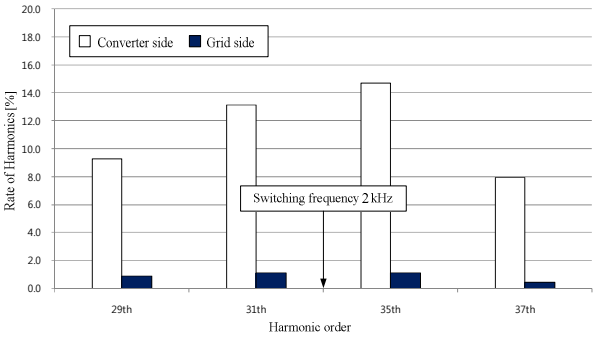

(b)

Fig. 13. The performance of the LCL-filter (a) Output currents of converter side (down) and grid side (up) and (b) Ripple rate spectra of the converter and grid currents.

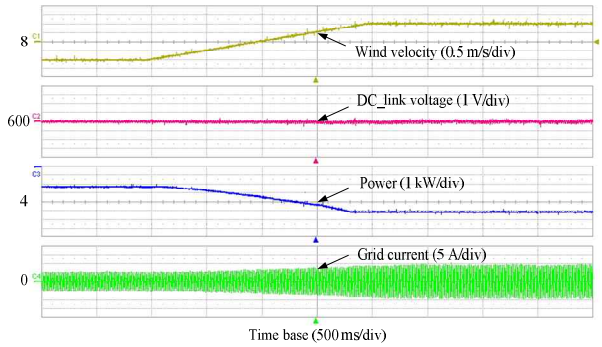

Fig. 14. The maximum power point tracking operation.

The blade torque was calculated from (4) and supplied to the induction motor drive through the communication link. Experiments were carried out to confirm the validity of the proposed design method. A picture of the actual experimental setup is shown in Fig. 12.

Fig. 13(a) shows the waveforms of the converter and grid currents when the wind speed was 9m/s. Fig. 13(b) shows the ripple rate of the converter and the grid currents. Although the total inductance of the designed LCL-filter was 15% of the L-filter, this LCL-filter was efficient in eliminating the harmonics of the grid current seen in Fig. 13(b). The total ripple factor of the 29th, 31th, 35th, and 37th order harmonics of the grid current was about 1.84% around switching frequency, as shown in Fig. 13(b). The value of the ripple factor in the design was 0.7%. The error of ripple factor was about 1.14% even though the total ripple factor was about 1.84% under 5kW of power. This result shows that the total ripple factor can be similar to the required ripple factor in Table 4 because the fundamental current increases by the magnitude of the rated current under 10kW of power, as shown in (9).

Fig. 14 shows that the generator operates at the maximum power point. When the wind speed increases from 7 to 9m/s, the torque of the generator follows the reference torque calculated by (5). The generated power and the grid current increased according to the change in the wind speed. The DC-link voltage is maintained at 600V. The experimental results demonstrate stable operation while using the proposed system and the validity of the proposed methods.

VII. CONCLUSION

This paper proposed a design method for the LCL-filter of a three-parallel power converter system for 2MW-wind turbines. The design method for the delta configured LCL-filters for this system and the compensation method to improve the power factor have been presented. A novel design method for the inner inductance of the LCL-filter was proposed in order to improve the accuracy of the design of the filter. Experimental results have shown that the switching harmonics, power factor, and stable MPPT-control performance have been improved.

ACKNOWLEDGEMENTS

This work was supported by KETEP (20114010203030) which is funded by MKE (Ministry of Knowledge Economy).

This work was supported by KETEP (G031462811) which is funded by MKE (Ministry of Knowledge Economy).

REFERENCES

[1] A. O. Di Tommaso, R. Miceli, G. Ricco Galluzzo, and M. Trapanese, "optimum performance of permanent magnet synchronous generators coupled to wind turbines," in *conf. Rec. IEEE PES2007*, pp. 1-7, Jun. 2007.

[2] Hae-Gwang Jeong, Hak-Sueng Roh, and Kyo-Beum Lee, "An improved maximum power point tracking method for wind power systems," *Energies*, pp. 1339-1354, May 2012.

[3] D. K. Yoon, H. G. Jeong, and K. B. Lee, "The design of an LCL-filter for the three-parallel operation of a power converter in a wind turbine," in *conf. Rec. IEEE ECCE2010*, pp. 1537-1544, Sep. 2010.

[4] K. W. Park and K. B. Lee, "Hardware simulator development for a 3-parallel grid-connected PMSG Wind power system," *Journal of Power Electronics,* Vol. 10, No. 5, pp. 555-562, Sep. 2010.

[5] Y. K. Kang, H. G. Jeong, and K. B. Lee, "Control method in a wind turbine driven by 3-parallel back-to-back converters using PQR power transformation," in *conf. Rec. IEEE IPEC2010*, pp. 2562-2568, Jun. 2010.

[6] Q. Zhang, L. Qian, C. Zhang, and D. Cartes, "Study on grid connected inverter used in high power wind generation system," in *conf. Rec. IEEE IAS2006*, pp. 1053-1058, Oct. 2006.

[7] T. M. Blooming, and D. J. Carnovale, "Application of IEEE Std. 519-1992 harmonic limits," *in conf. Rec. IEEE IAS2006*, pp. 1-9, Oct. 2006.

[8] I. J. Gabe, V. F. Montagner, and H. Pinheiro, "Design and implementation of a robust current controller for vsi connected to the grid through an LCL filter," *IEEE Trans. Power Electron.*, Vol. 24, No. 6, pp. 1444-1452, Jun. 2009.

[9] H. G. Jeong, K. B. Lee, S. W. Choi, and W. J. Choi, "Performance improvement of LCL-Filter-Based grid-connected inverters using PQR power transformation," *IEEE Trans. Power Electron.*, Vol. 25, No. 5, pp. 1320-1330, May 2010.

[10] M. Liserre, A. Dell'Aquila, and F. Blaabjerg, "Genetic algorithm based design of the active damping for a LCL-filter three-phase active rectifier," *IEEE Trans. Power Electron.*, Vol. 19, No. 1, Jan. 2004.

[11] M. Liserre, F. Blaabjerg, and S. Hansen, "Design and control of an LCL-filter-based three-phase active rectifier," *IEEE Trans. Ind. Appl.*, Vol. 41, No. 5, pp. 1284-1285, Sep./Oct. 2005.

[12] K. Jalili, S. Bernet, "Design of filters of active-front-end two-level voltage-source converters," *IEEE Trans. Ind. Electron.*, Vol. 56 , No. 5, pp. 1674-1689, May 2009.

[13] X. Guo, X. You, X. Li, R. Hao, and D. Wang, "Design method for the LCL filters of three-phase voltage source PWM rectifiers," *Journal of Power Electronics*, Vol. 12, No. 4, Jul. 2012.

[14] R. Öten and R. J. P. de Figueiredo, "An efficient method for L-filter design," *IEEE Trans. Signal Process.*, Vol. 51, No. 1, Jan. 2003.

Hae-Gwang Jeong was born in Jeonju, Korea, in 1982. He received his B.S. in Electrical Engineering from Chonbuk National University, Jeonju, Korea, in 2008. He received his M.S. from the Department of Electrical and Computer Engineering, Ajou University, Suwon, Korea, in 2010. He is currently working toward his Ph.D. at Ajou University. His current research interests include power conversion, grid connected inverters and renewable energy.

Dong-Keun Yoon was born in Daejeon, Korea, in 1983. He received his B.S. from Chonbuk National University, Jeonju, Korea, in 2009. He received his M.S. from the Department of Electrical and Computer Engineering, Ajou University, Suwon, Korea, in 2011. Currently he is working for the Research Group of LG Innotek Co., Ltd., Ansan, Korea.

Kyo-Beum Lee was born in Seoul, Korea, in 1972. He received his B.S. and M.S. in Electrical and Electronic Engineering from Ajou University, Suwon, Korea, in 1997 and 1999, respectively. He received his Ph.D. in Electrical Engineering from Korea University, Seoul, Korea, in 2003. From 2003 to 2006, he was with the Institute of Energy Technology, Aalborg University, Aalborg, Denmark. From 2006 to 2007, he was with the Division of Electronics and Information Engineering, Chonbuk National University, Jeonju, Korea. In 2007 he joined the School of Electrical and Computer Engineering, Ajou University, Suwon, Korea. He is an Associated Editor of the IEEE Transactions on Power Electronics, the IEEE Transactions on Industrial Electronics, and the Journal of Power Electronics. His current research interests include electric machine drives and renewable power generation.